Applied Catalysis B: Environmental 117–118 (2012) 321–329

Contents lists available at SciVerse ScienceDirect

Applied Catalysis B: Environmental

journal homepage: www.elsevier.com/locate/apcatb

RuSn bimetallic catalysts for selective hydrogenation of levulinic acid to γ-valerolactone

Stephanie G. Wettstein[a], Jesse Q. Bond[a], David Martin Alonso[a], Hien N. Pham[b], Abhaya K. Datye[b], James A. Dumesic[a,*]

[a] Department of Chemical & Biological Engineering, University of Wisconsin-Madison, Madison, WI 53706, USA
[b] Department of Chemical & Nuclear Engineering and Center for Microengineered Materials, University of New Mexico, Albuquerque, NM 87131, USA

ARTICLE INFO

Article history:
Received 31 October 2011
Received in revised form 23 January 2012
Accepted 27 January 2012
Available online 5 February 2012

Keywords:
Alkylphenol
Biomass
Heterogeneous catalysis
Renewable resources
Bimetallic

ABSTRACT

Carbon-supported ruthenium catalysts containing different amounts of tin were studied for the hydrogenation of levulinic acid (LA) to gamma-valerolactone (GVL) in a 2-sec-butyl-phenol (SBP) solvent. Results from reaction kinetics measurements (453 K and 35 bar H_2) showed that the Ru/C catalyst was initially more active for hydrogenation of both LA and SBP (i.e., 0.051 s^{-1} for conversion of LA to GVL), followed by continuous deactivation versus time on stream. In contrast, the catalyst containing equal amounts of Ru and Sn had a lower activity for LA to GVL conversion (0.005 s^{-1}), but displayed stable activity versus time on stream and showed 100% selectivity for hydrogenation of LA versus the SBP solvent. Increasing the amount of Sn to a 1 to 4 Ru:Sn atomic ratio creates an additional phase, β-Sn, that is not active for hydrogenation, leaches into the SBP solvent, and sinters under reaction conditions. Results from CO and O_2 chemisorption and electron microscopy measurements indicated that the Ru-based metal particles did not leach or sinter at reaction conditions, and that the surfaces of these particles became progressively enriched with Sn as the Sn-loading increases. In addition, Sn did not significantly leach from the catalysts when present as an intermetallic alloy with Ru, such as Ru_2Sn_3 and Ru_3Sn_7. Using LA produced from corn stover, the $RuSn_4$/C catalyst was stable and demonstrated that it is a promising catalyst to produce valuable chemicals and fuels from real biomass.

© 2012 Elsevier B.V. All rights reserved.

1. Introduction

Recent research has focused on the production of lignocellulosic platform molecules that can be converted into a broad range of fuels and chemicals. For example, γ-valerolactone (GVL) has attracted considerable attention [1–6] because high yields can be achieved through hydrogenation of levulinic acid (LA) [1] using heterogeneous catalysts [7,8] for which production methods are available [9,10]. As a pure product, GVL may be used as solvent or blended with conventional gasoline in a capacity similar to ethanol [11]. In addition, GVL can be converted into a variety of chemicals, such as, 1,4 pentanediol [12], α-methylene γ-valerolactone [13], or pentenoate esters [14]. Furthermore, GVL can be used as precursor of gasoline and diesel fuels, such as C_8–C_{16} alkenes [15], C_9–C_{18} alkanes [2], C_9 alkanes [1], valeric esters [16], or butene isomers [17,18].

The production of LA typically employs treatment of cellulose in dilute (0.1–0.5 M) solutions of sulfuric acid (SA) [9]; however, the presence of SA negatively impacts downstream catalytic processes, in particular those involving metal catalysts, such as Ru. The production of LA using solid acid catalysts [19,20] would allow for simple separation of the acid catalyst from the aqueous feed, but LA yields are not competitive with those obtained from reactions catalyzed by SA. Therefore, SA must be either neutralized or removed through combined solvent extraction and distillation [21], with the latter step being preferred in the interest of resource conservation.

We recently described a solvent extraction method using 2-sec-butylphenol (SBP) to recover LA from aqueous solutions of SA [22]. The extracted LA sequentially underwent selective hydrogenation to yield GVL using a RuSn catalyst to minimize the hydrogenation of SBP. In the present paper, we consider the intrinsic activity, selectivity, and stability of various Ru_xSn_y/C catalysts, with particular emphasis on the effect of adding Sn to the Ru/C catalyst. In addition, we report results from characterization studies of fresh and spent catalysts to provide insights into the nature of the active catalyst and possible sources of catalyst deactivation. Importantly, we demonstrate that addition of Sn stabilizes Ru/C, even in the presence of feed streams derived from real biomass, e.g., corn stover.

* Corresponding author. Tel.: +1 608 262 1095; fax: +1 608 262 5434.
E-mail address: dumesic@engr.wisc.edu (J.A. Dumesic).

0926-3373/$ – see front matter © 2012 Elsevier B.V. All rights reserved.
doi:10.1016/j.apcatb.2012.01.033

2. Experimental

2.1. Catalyst preparation

A 5 wt% Ru/C catalyst (Sigma–Aldrich) was used in this study for LA hydrogenation and for preparation of Ru_xSn_y bimetallic catalysts. The Ru_xSn_y/C samples were prepared by incipient wetness impregnation of 5 wt% Ru/C with an aqueous solution of $SnCl_2{\cdot}2H_2O$, followed by heating in air at 353 K for 2 h. Prior to reactions in fixed bed reactors, catalyst samples were reduced in situ for 3 h at 723 K (1 K min^{-1}). When exposure to air was necessary, catalyst samples were reduced as described above, and subsequently passivated in 2% O_2 in He (50 cm^3 min^{-1}, Airgas) at 298 K for 60 min prior to exposure to ambient conditions. Monometallic Sn/C samples were synthesized by incipient wetness impregnation of Norit SX 1G with an aqueous solution of $SnCl_2{\cdot}2H_2O$, followed by heating in air 2 h at 353 K, and reduction in H_2 (3 h at 723 K).

2.2. X-ray diffraction

X-ray diffraction (XRD) was used to probe interactions between Ru and Sn and to provide information regarding metal particle size. Powder diffraction was carried out using a Rigaku Rapid II with a molybdenum source. Prior to XRD studies, Ru_xSn_y/C catalysts were reduced in flowing H_2, and passivated in flowing 2% O_2 in He. Samples were crushed to a uniform size and loaded into a 0.5 mm borosilicate capillary for analysis.

2.3. Transmission electron microscopy (TEM)

Catalyst samples for TEM measurements were dispersed in ethanol using a mortar and pestle, then mounted on carbon coated Cu grids followed by slow evaporation of the solvent at ambient conditions for examination in a transmission electron microscope (TEM; JEOL 2010F) equipped with an Oxford energy dispersive spectroscopy (EDS) system for elemental analysis. Images were recorded in bright field high resolution (HRTEM) mode as well as in high angle annular dark field (HAADF) mode. A LaB_6 filament at 200 kV was used as the electron beam source. The average particle size was calculated by measuring the diameter of over 1000 particles from multiple TEM images of different grid areas.

2.4. Scanning electron microscopy/electron dispersive spectrometry

A Hitachi S-5200 scanning electron microscope (SEM) equipped with an EDS from Princeton Gamma Tech was operated at 2 kV to image the samples in secondary electron and backscattered modes. For EDS, 15 kV was used for spotlighting and box analysis. For sample preparation, the catalyst was pressed onto carbon double-sided tape that had been attached to an aluminum sample holder.

2.5. Temperature programmed reduction

Temperature programmed reduction (TPR) was performed on dried Ru/C, Sn/C, and Ru_xSn_y/C samples using a residual gas analyzer (RGA) with a quadrupole mass spectrometer (Stanford Instruments, RGA 200). Prior to TPR measurements, the cell volume was purged by flowing helium (50 cm^3 min^{-1}, Airgas, UHP grade) for 30 min at 298 K. The inlet gas feed was then switched to 5% H_2 in N_2 (50 cm^3 min^{-1}, Airgas) and held at 298 K until a stable baseline signal was achieved, before increasing the temperature at a rate of 10 K min^{-1} to 973 K.

2.6. Physisorption

Fresh Ru_xSn_y/C samples were characterized by adsorption–desorption N_2 isotherms, collected using a Micromeritics ASAP 2020 system, to determine catalyst surface area and pore volume. Prior to analysis, catalyst samples were degassed under vacuum at 373 K in He for 12 h. The physisorption was measured at liquid N_2 temperatures. Physisorption measurements on spent samples (i.e., used for reaction kinetics studies) were carried out by first washing the spent catalysts with acetone (to remove residual non-volatile organic species (SBP)), followed by drying. A reduced and passivated sample (fresh) was washed and dried to ensure that the surface area was not affected by the washing procedure. Surface areas were determined using the BET method. Pore volumes were determined from the adsorption branch of the N_2 isotherm at $P/P_0 = 0.97$ single point.

2.7. Chemisorption

Fresh Ru_xSn_y/C samples were characterized by volumetric titration of exposed metal sites with CO and O_2 chemisorption (Micromeritics ASAP 2020). Prior to analysis, catalyst samples were outgassed under vacuum at 303 K and subsequently reduced in flowing H_2 for 4 h at 723 K (80 cm^3(STP) min^{-1} H_2, 1.3 K min^{-1}). The sample was then evacuated at 723 K for 60 min to remove adsorbed H_2 and finally cooled to 303 K. CO chemisorption was measured at 303 K. To limit the extent of bulk Ru oxidation [23] and the potential formation of volatile RuO_4 [24], O_2 chemisorption was determined at 195 K. Chemisorption measurements on samples that had been used for reaction kinetics studies (453 K, 35 bar, 300 h on stream) were carried out by first washing the spent catalysts with acetone (to remove residual non-volatile organic species (SBP)), followed by drying under vacuum and sifting through a sieve to remove residual quartz fibers and granules. Samples were subsequently placed in a quartz chemisorption cell and analyzed according to the above protocol.

2.8. Studies of catalytic activity and stability

The activity and selectivity of each catalyst was measured for the hydrogenation of LA in SBP. Reactions were carried out in a fixed bed reactor in an up-flow configuration as described previously [22]. The catalyst was reduced in situ for 3 h at 723 K (1 K min^{-1}) before use. Feeds for catalytic experiments were prepared by adding commercial LA (Sigma–Aldrich, 98%) to SBP (Alfa-Aesar, >98%). The LA feed from corn stover was prepared as indicated elsewhere [22]. Gas phase products were analyzed using a GC-2014 (Shimadzu) equipped with an FID and a GC-8A (Shimadzu) with a TCD. Liquid samples were analyzed using a GC-2010 (Shimadzu) with an FID and an RTx-5 column. Qualitative identification of products was achieved using GC–MS (Shimadzu GCQP-2010). For the data reported herein, total and individual mass balances for each compound were within 5%.

In this study, both hydrogenation of LA to GVL and hydrogenation of SBP to butyl cyclohexanol/butyl cyclohexanone were observed. The hydrogen consumption selectivity for a given catalyst is thus defined according to Eq. (1):

$$S_i = \frac{\xi_i}{\sum \xi_i} \times 100 \quad (1)$$

where ξ_i represents the percent of hydrogen consumed to hydrogenate the LA and SBP. In general, the LA hydrogenation proceeds to GVL with selectivities >99%, while SBP hydrogenation results in the formation of sec-butyl cyclohexanol and sec-butyl cyclohexanone with selectivities >99%. The hydrogen consumption selectivity

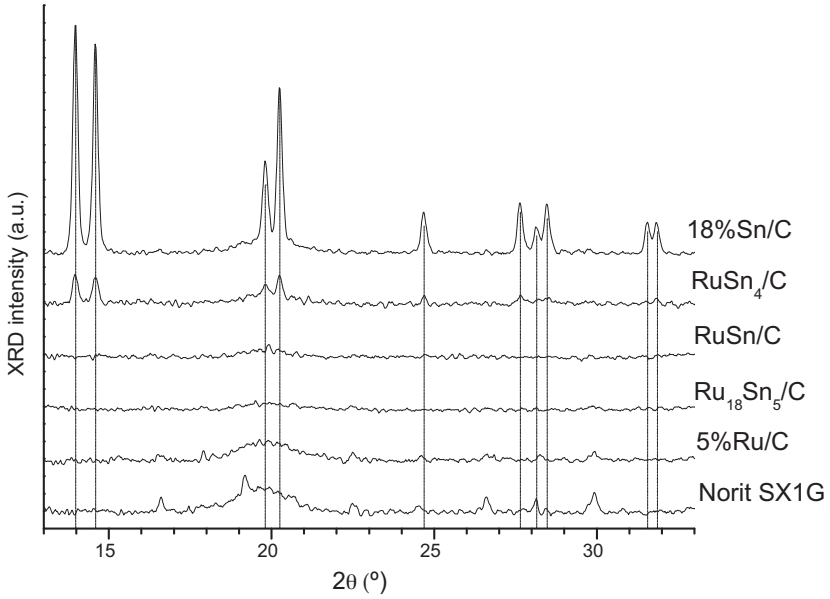

Fig. 1. XRD patterns of Ru_xSn_y/C catalysts after reduction at 723 K in H_2.

reported herein compare the relative extents to which specific materials catalyze LA and SBP hydrogenation.

3. Results

3.1. Characterization

3.1.1. X-ray diffraction

As seen in the XRD patterns in Fig. 1, no Ru phase is observed in the reduced Ru/C sample, indicating the presence of nanoparticles that are too small to be resolved by XRD (less than 4 nm) [25]. In addition, no reflections were observed for $Ru_{18}Sn_5$/C and RuSn/C samples (1.6 and 5.5 wt% Sn, respectively), again indicating well-dispersed metal particles. In contrast, the 18% Sn/C sample had a well defined diffraction pattern, corresponding to metallic Sn (vertical lines, Fig. 1, PDF 4-673). According to the Scherrer equation, the size of the Sn particles was on the order of 100 nm. Thus, using $SnCl_2{\cdot}2H_2O$ as a precursor in the absence of Ru nanoparticles, extensive sintering of the Sn phase occurred upon reduction at 723 K. For the Sn-rich sample, $RuSn_4$/C, a distinct Sn phase was observed, suggesting the Sn segregated into large clusters, which was confirmed by TEM and EDS (Section 3.1.2). As with the monometallic Sn/C sample, metal particle sizes are estimated to be on the order of 100 nm by the Scherrer equation, and confirmed by TEM. The diffraction feature observed at 20° 2θ, was present in all samples and is attributable to the carbon support (see XRD pattern for untreated Norit SX1G, Fig. 1).

3.1.2. TEM/SEM

The TEM and SEM images confirmed that the metal particles were well dispersed for the $Ru_{18}Sn_5$/C and RuSn/C catalyst samples (Fig. 2a and b) after reduction (723 K), and the majority of particles were smaller than 5 nm. In contrast, the sample with the highest loadings of Sn, $RuSn_4$/C, showed a mixture of small metal particles and large metal clusters exceeding 100 nm in diameter (bright spots, Fig. 2c).

The large particles in the $RuSn_4$/C sample were not observed prior to reduction (Fig. 3a); however, upon reduction at 723 K, Fig. 3b, large clusters of metal particles were visible, indicating that $RuSn_4$/C particles sintered at temperatures required for reduction of $SnCl_2$. This sintering behavior was not observed for samples with lower Sn loadings. Analyses using EDS of the large particles in the $RuSn_4$/C (Fig. 3b) indicated that the metal compositions ranged from 93 to 97 wt% Sn (1:14–1:42 Ru:Sn atomic ratio), with the proportion of Sn increasing with particle size. The 18 wt% Sn/C catalyst showed a similar behavior; prior to reduction, large metal particles were not observed in the catalyst (Fig. 3c), whereas particles larger than 500 nm were formed due to sintering (Fig. 3d) during reduction and passivation.

3.1.3. Temperature programmed reduction

Fig. 4 shows reduction profiles for various Ru_xSn_y/C catalysts and for Ru/C, which has a maximum rate of reduction at approximately 400 K and is consistent with prior reports [21]. High temperature consumption of H_2 over the Ru/C sample (500–800 K) was attributed to methane formation (confirmed by

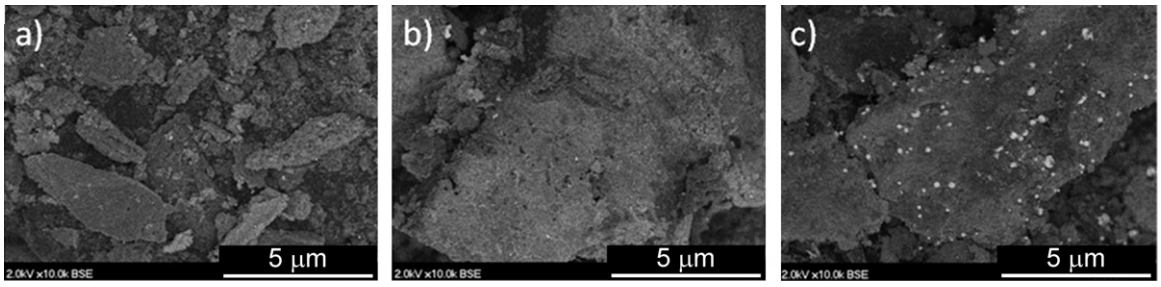

Fig. 2. Back-scattered SEM images of (a) $Ru_{18}Sn_5$/C, (b) RuSn/C, and (c) $RuSn_4$/C after reduction and passivation at 723 K.

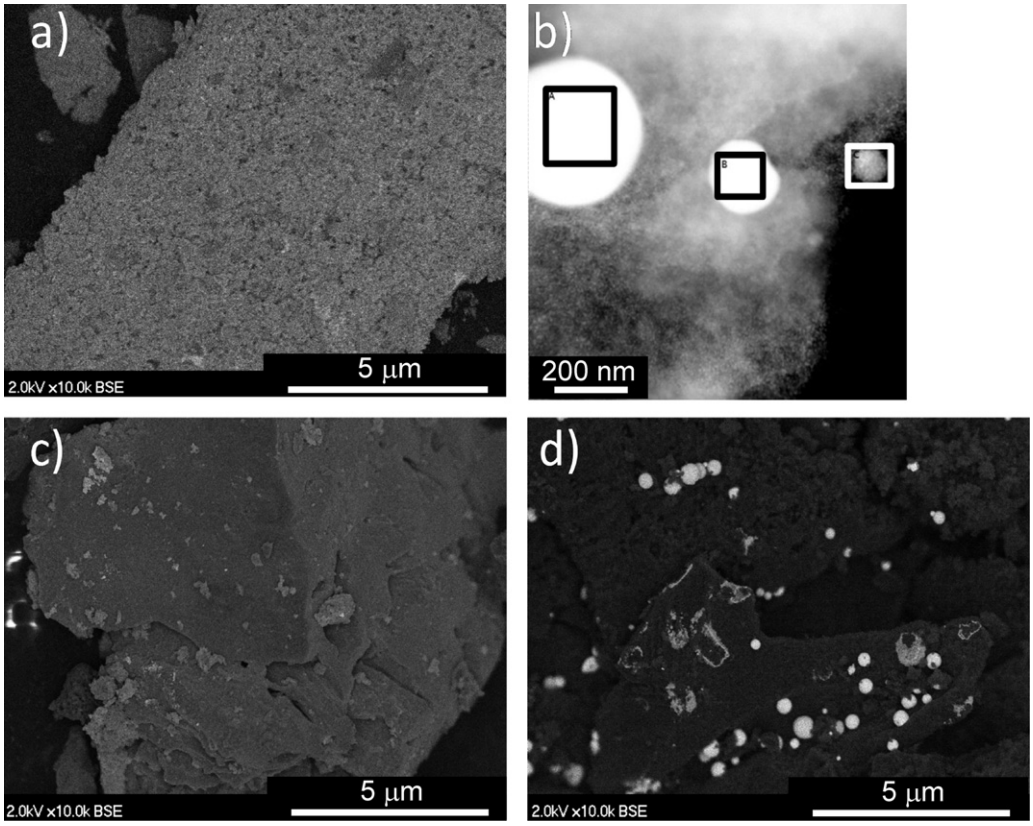

Fig. 3. Back-scattered SEM image after synthesis and 2 h in 368 K oven of (a) $RuSn_4$/C and (c) pure Sn/C. (b) TEM image of $RuSn_4$/C and (d) SEM image of pure Sn/C after reduction at 723 K and passivation at 303 K.

mass spectrometry) arising through reduction of functionalized carbon on the catalyst support. Methane formation was observed primarily over the Ru/C catalyst and was less evident for samples containing Sn. In contrast to RuO_x, the $SnCl_2$ used to prepare the Ru_xSn_y samples was less readily reduced, evidenced by a maximum reduction temperature of 723 K for the monometallic 18% Sn/C sample. For this sample, the observed region of H_2 uptake was broad, beginning at 573 K and continuing through 873 K. Consumption of H_2 in this region was attributed to reduction of $SnCl_2$ to form Sn^0 and HCl. Compared to monometallic Ru/C, as the Sn content increased, the primary reduction peak shifted to higher temperatures, and a high temperature shoulder on the main peak appeared. In general, this shift of the primary reduction peak was qualitatively consistent with prior TPR results for $Ru_xSn_yB_z$ supported on Al_2O_3 [26]; however, previously reported reduction temperatures are higher, which is likely attributable to the oxide support. The diminished H_2 consumption at temperatures below 400 K for Sn-rich samples was associated with a decrease in surface Ru, and was consistent with results from CO chemisorption.

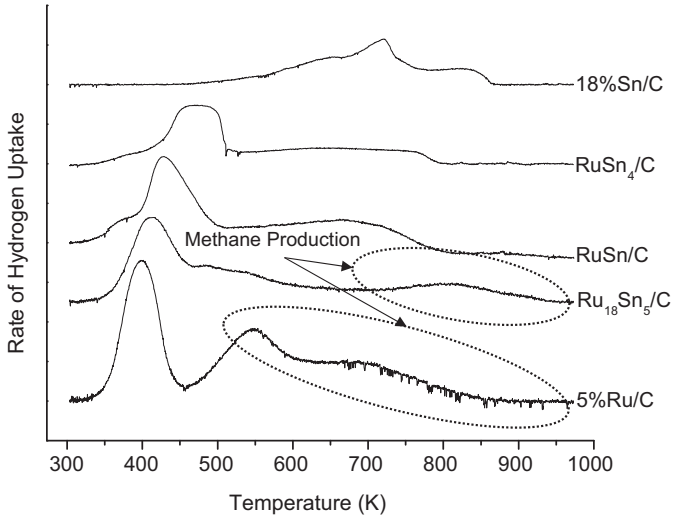

Fig. 4. Reduction profiles for Ru_xSn_y/C catalysts. Rate of hydrogen uptake is normalized by total metal sites.

The high temperature shoulder for $Ru_{18}Sn_5$/C can be attributed to the reduction of Sn^{2+} species by H_2 spillover from surface Ru. The temperature for Sn^{2+} reduction (460–600 K) was substantially lower than that observed for bulk $SnCl_2$ on carbon (573–873 K), suggesting that Sn particles exist in close contact with Ru particles in the $Ru_{18}Sn_5$/C sample. The high temperature shoulders on the primary reduction peaks for the RuSn/C and $RuSn_4$/C samples were broadened substantially compared to the $Ru_{18}Sn_5$/C sample, beginning at 500 K and extending to 750–800 K. This temperature range for H_2 uptake coincided with the reduction temperature for the monometallic Sn/C, and indicates the presence of isolated, Sn-enriched metal clusters that are not in close proximity to Ru atoms and therefore, were not reduced through H_2 spillover. Similar trends were reported previously by Aguirre et al. for Rh_xSn_y/SiO_2 catalysts [27].

3.1.4. Chemisorption and physisorption measurements

Previous research has demonstrated that CO does not adsorb irreversibly on metallic Sn, ionic Sn, or noble metal particles decorated or encapsulated by Sn [28]; therefore, CO uptake is an indicator of surface Ru sites while O_2 chemisorption is an indicator of the total metal sites. Table 1 shows that the addition of Sn decreases the CO uptake, which can be attributed to a surface

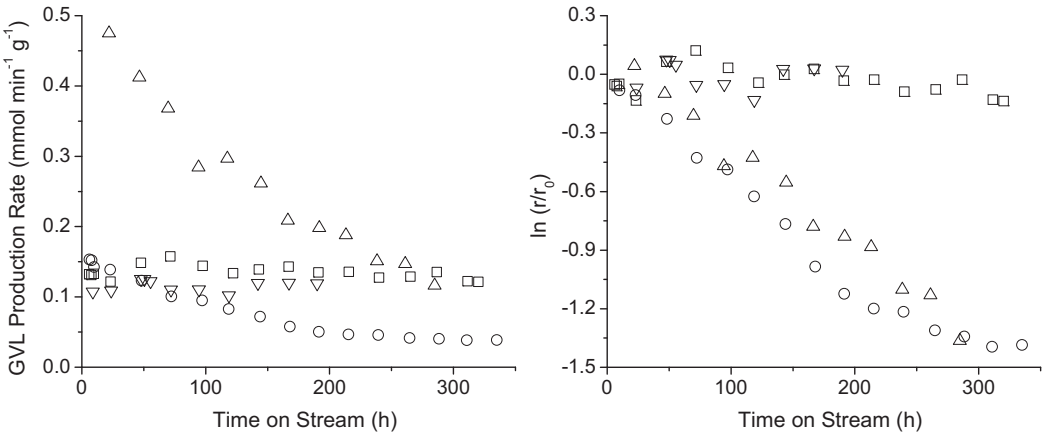

Fig. 5. Rates of GVL production over various Ru_xSn_y/C samples with time on stream. Production rates of GVL normalized by: (a) catalyst mass and (b) initial rate. Ru/C (△), $Ru_{18}Sn_5$/C (○), RuSn/C (▽), $RuSn_4$/C (□). WHSV = 1.2 h^{-1} (3.6 h^{-1} for Ru/C), 453 K, and 35 bar H_2.

enriched in Sn and/or Ru_xSn_y phases that do not bind CO irreversibly. Accordingly, the general trend of diminished CO uptake with addition of Sn indicates that the quantity of surface Ru sites continuously decreases from 126 μmol g^{-1} for the monometallic Ru/C catalyst to less than 1 μmol g^{-1} for the $RuSn_4$/C catalyst. Physisorption measurements using N_2 showed that the reduced and passivated $RuSn_4$ catalyst had slightly lower surface area and pore volume than the other catalysts, which is attributed to the high Sn loading in this sample.

The O_2 uptake increased with total metal loading for samples containing Ru (Table 1), and indicates that the decrease in CO uptakes for samples with larger amounts of Sn was not caused by a loss of metal dispersion, but by suppression of CO binding at Sn-enriched surfaces. The extent of O_2 adsorption increased with Sn loading, and uptakes are approximately 0.2–0.4 μmol O_2/μmol metal. Both the $Ru_{18}Sn_5$/C (0.29 μmol O_2/μmol metal) and Ru/C (0.30 μmol O_2/μmol metal) catalysts have similar metal dispersion, while the RuSn/C catalyst has a slightly higher metal dispersion (0.41 μmol O_2/μmol metal). Further increasing the Sn content to $RuSn_4$/C caused a decrease in metal dispersion (0.24 μmol O_2/μmol metal), indicating the formation of large, Sn-rich aggregates, which was confirmed by TEM. The monometallic Sn/C sample, at Sn loadings equivalent to the $RuSn_4$ catalyst, had a substantially lower metal dispersion (0.009 μmol O_2/μmol metal), which indicates sintering due to the low melting point of Sn (505 K) and the high temperature required for reduction of the $SnCl_2$ precursor (723 K, see Section 3.1.3).

3.2. Reaction kinetics studies

3.2.1. Catalyst activity

The addition of Sn to Ru/C decreased the rates of hydrogenation for both LA and SBP (Table 2). Table 2 reports the initial rates at 453 K of LA and SBP hydrogenation expressed both per gram of catalyst and as turn-over frequencies (TOF), which were calculated using the number of surface sites determined by O_2 chemisorption. Monometallic Ru/C has the highest intrinsic activity for hydrogenation of both LA (0.051 s^{-1}) and SBP (0.015 s^{-1}) when compared to Ru_xSn_y bimetallics. The decrease in catalytic activity seen with the bimetallic catalysts coincided with an increase in H_2 consumption selectivity for the conversion of LA (C=O hydrogenation) as opposed to SBP (aromatic hydrogenation). To verify that the improvement in selectivity was not associated with lower LA conversion, some experiments were carried out at 100% LA conversion; the selectivity increased with time on stream, indicating that H_2 consumption selectivity is not related to conversion, but to catalyst deactivation. Adding a small amount of Sn ($Ru_{18}Sn_5$/C, 1.6 wt% Sn) decreased the activity for both LA and SBP hydrogenation to 0.014 s^{-1} and 0.005 s^{-1}, respectively, but the H_2 consumption selectivity remained similar to Ru/C for LA hydrogenation (73%). This result agrees with the CO chemisorption studies, where $Ru_{18}Sn_5$/C irreversibly binds 101 μmol CO g^{-1} (Table 1), and has a Ru surface concentration comparable to 5% Ru/C (126 μmol CO g^{-1}). Thus, the $Ru_{18}Sn_5$/C catalyst still had surface Ru atoms that were responsible for the initial activity and selectivity.

As the Sn content of the catalyst increased, the initial LA turnover frequency decreased to 0.005 s^{-1} for both RuSn/C and $RuSn_4$/C. At this point, hydrogenation of SBP was completely suppressed and only hydrogenation of the C=O bond in the LA was observed. The low LA hydrogenation rate, in conjunction with minimal CO uptake (Table 1), indicates that Ru ensembles comprise a small fraction of the total site density and are not substantial contributors to the initially observed activity for either of these catalysts. Equimolar loadings of Ru and Sn appeared sufficient to entirely eliminate hydrogenation of SBP (at 80% LA conversion), suggesting that at this loading and beyond, large ensembles of Ru atoms comprised an insignificant portion of surface metal sites, and the observed activity and selectivity arose because of Ru–Sn interactions.

Table 1
Comparison of CO and O_2 uptakes on fresh and spent Ru_xSn_y/C catalysts.

Sample	Nominal Ru loading (μmol g^{-1})	Nominal Sn loading (μmol g^{-1})	Fresh CO uptake (μmol g^{-1})	μmol CO/μmol total metal	Spent CO uptake (μmol g^{-1})	Fresh O_2 uptake (μmol g^{-1})	μmol O_2/μmol total metal	Spent O_2 uptake (μmol g^{-1})
5% Ru/C	495	0	126	0.26	46	150	0.30	78
$Ru_{18}Sn_5$/C	487	135	101	0.16	27	179	0.29	154
RuSn/C	467	467	21	0.02	13	379	0.41	179
$RuSn_4$/C	401	1600	0.8	0.0004	15	474	0.24	270
18% Sn/C	0	1700	–	–	–	15	0.009	–

Table 2
Initial hydrogenation rates observed for various Ru_xSn_y/C samples. T = 453 K, feed = 2 M LA in SBP. H_2 flow rate is 25 cm^3(STP) min^{-1}, WHSV = 3.6 h^{-1} (Ru/C) and 1.2 h^{-1}(all others).

Catalyst	LA hydrogenation rate (μmol min^{-1} g^{-1})	SBP hydrogenation rate (μmol min^{-1} g^{-1})	LA TOF (s^{-1})	SBP TOF (s^{-1})	LA hydrogenation selectivity (%)
Ru/C	455	140	0.051	0.015	77
$Ru_{18}Sn_5$/C	154	56	0.014	0.005	73
RuSn/C	116	0	0.005	–	100
$RuSn_4$/C	139	0	0.005	–	100

3.2.2. Catalyst stability

Stability with respect to time on stream of the Ru/C and Ru_xSn_y/C catalysts during hydrogenation of LA in SBP is important for the practical production of GVL. Both the activity and the selectivity toward LA conversion (as opposed to SBP conversion) varied with time on stream for Ru-rich catalysts. Importantly, the Sn-rich catalysts demonstrated more stable activity versus time on stream (Fig. 5a). The initial rate of GVL production over Ru/C was 4–5 times higher than the rates observed on any of the bimetallic catalysts; however, the Ru/C catalyst deactivated continuously over the course of 300 h on stream, with a first order deactivation constant of 0.0052 h^{-1}. Additionally, the selectivity for conversion of LA increased (Fig. 6) with time on stream as the catalyst deactivates, but some SBP hydrogenation was always observed. In addition, the initial catalytic activity could not be restored by treatment in H_2 at the initial reduction temperature (723 K), suggesting that the deactivation of the catalyst (on a carbon support) was irreversible.

The initial GVL production rate for the $Ru_{18}Sn_5$/C catalyst was 154 μmol min^{-1} g^{-1}, and the rate decreased for approximately 200 h on stream, and then stabilized at 37 μmol min^{-1} g^{-1} (Fig. 5a). For the first 200 h of reaction, the rate of deactivation was first order with a deactivation constant of 0.0060 h^{-1} (Fig. 5b), which is comparable to that observed for monometallic Ru/C. Similar to the Ru/C catalyst, the initial selectivity for LA hydrogenation increased with time on stream as the catalytic activity stabilized; however, the $Ru_{18}Sn_5$/C catalyst achieved 100% LA selectivity after the deactivation period. Bimetallic samples with higher Sn loadings (RuSn/C and $RuSn_4$/C) exhibited initial hydrogenation rates of 116 and 139 μmol min^{-1} g^{-1}, respectively (Fig. 5a), and showed no evidence of deactivation (Fig. 5b). In addition, no hydrogenation of SBP was observed, indicating that surface metal sites were primarily formed from Ru and Sn in close contact, which is supported by CO and O_2 chemisorption.

Due to the stability of the $RuSn_4$/C catalyst, it was studied for the hydrogenation of LA produced from corn stover, and Fig. 7 shows that the GVL production rate was stable over more than 140 h on stream, which indicates that the presence of by-products from LA production, such as formic acid and other impurities arising from biomass deconstruction, did not affect the stability of the catalyst. The formic acid decomposed to CO_2 and H_2 with >99% selectivity over the $RuSn_4$/C catalyst, and could possibly be used as an internal source of H_2.

3.3. Characterization of post-reaction catalyst samples

3.3.1. TEM/EDS

Fig. 8 shows that, prior to reaction, metal particles were well dispersed for reduced samples of Ru/C (a1), $Ru_{18}Sn_5$/C (b1), and RuSn/C (c1). Although the overall atomic ratio of the $RuSn_4$/C catalyst is 1:4, this catalyst (Fig. 8d1) had large clusters of metal that were mostly comprised of Sn (1:14–1:42 Ru:Sn atomic ratio) and smaller particles with Ru:Sn ratios varying between 1:2 and 1:4. Post reaction samples (Fig. 8a2–d2) showed that the only catalyst with significant particle size changes was the $RuSn_4$/C bimetallic catalyst, which had metal particles with compositions in the range of 1:2 Ru:Sn atomic ratio. This change in Ru:Sn ratio indicates that Sn leached from the catalyst during reaction, resulting in a surface close to the RuSn/C catalyst within the error of the measurements (Fig. 9).

EDS analyses for Ru/C, $Ru_{18}Sn_5$/C, and RuSn/C showed a decrease in the bulk mass loadings of Sn (Fig. 9), which was accompanied by a decrease in the O_2 uptakes observed in the chemisorption measurements (Table 1). The loading of the Ru/C catalyst was not significantly different before and after reaction. For the RuSn/C catalyst, ICP analysis of fresh and spent samples by Galbraith Laboratories suggested a small decrease in Ru content (≈10%) after 300 h on stream. This small reduction

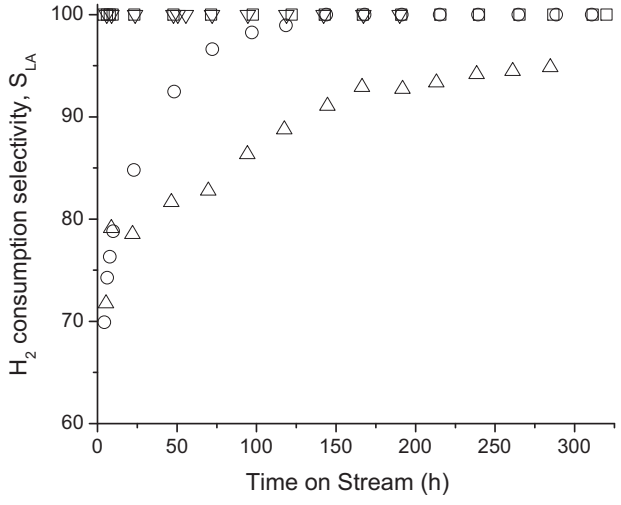

Fig. 6. Hydrogenation selectivity observed for Ru_xSn_y/C samples with time on stream. Ru/C (△), $Ru_{18}Sn_5$/C (○), RuSn/C (▽), $RuSn_4$/C (□). WHSV = 1.2 h^{-1} (3.6 h^{-1} for Ru/C), 453 K, and 35 bar H_2.

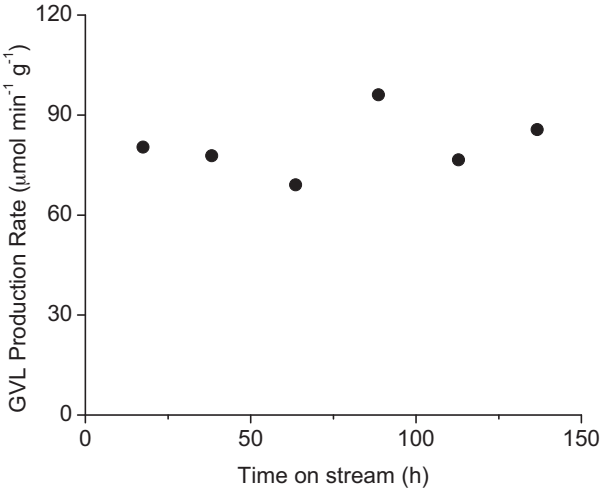

Fig. 7. GVL production rate versus time on stream for LA produced from corn stover on a $RuSn_4$/C catalyst, at a WHSV = 0.8 h^{-1}, 493 K, and 35 bar H_2.

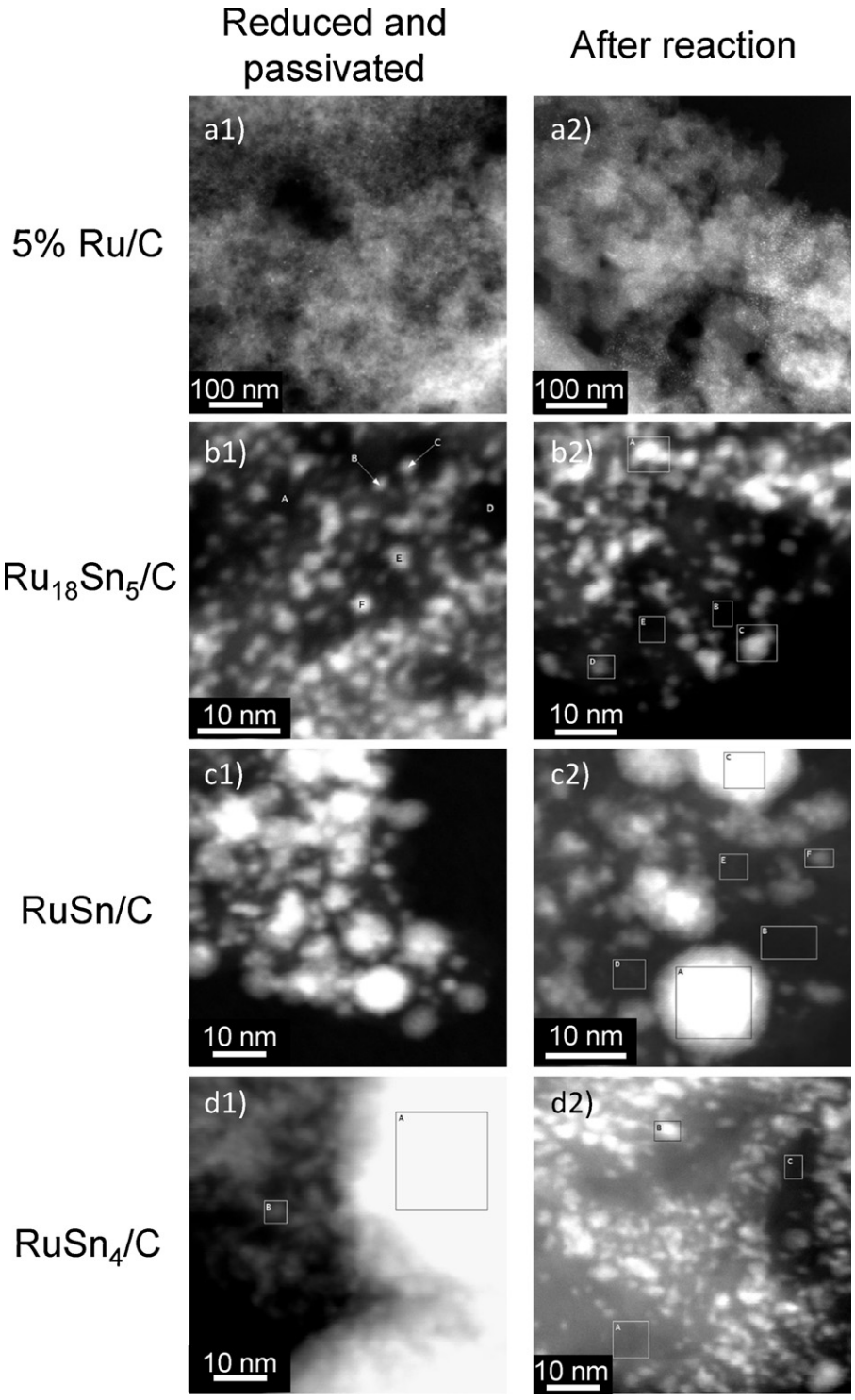

Fig. 8. HAADF TEM images of (a) 5% Ru/C, (b) $Ru_{18}Sn_5/C$, (c) RuSn/C, and (d) $RuSn_4/C$ after reduction and passivation at 723 K, a1–d1 and after reaction, a2–d2. Note that the 5% Ru/C is at a lower magnification than the others.

in Ru content was not sufficient to explain the loss in activity, and was likely associated with contamination of the spent samples (e.g., adsorbed solvent and possible coking). Coking of the catalysts appeared to be a contributor to catalyst deactivation, because only a fraction of the catalytic activity was restored when the deactivated catalyst was subjected to a regeneration cycle (reduction in H_2 (50 cm^3 min^{-1} (STP)) at 723 K for 3 h).

3.3.2. Physisorption and chemisorption measurements

Results from chemisorption measurements on spent samples (Table 1) revealed a substantial decrease in both CO and O_2 uptake in catalyst samples recovered from flow reactors after 300 h on stream. A lower active site density (63% decrease in CO uptake) in the case of Ru/C was consistent with the 73% observed decrease in catalytic activity. As with the fresh catalyst samples, O_2 uptake was higher than CO uptake, although a 48% decrease in O_2 indicates a

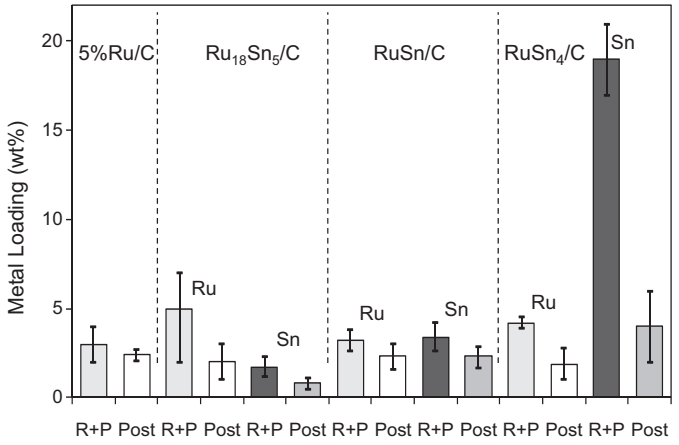

Fig. 9. Metal loadings determined by EDS (with 95% confidence limits) for reduced and passivated and for post reaction catalysts.

loss of accessible metal sites after subjecting the catalyst to typical reaction conditions.

The hydrogenation activity of the $Ru_{18}Sn_5$/C catalyst after 300 h was 76% lower than the initial activity. This loss agreed with a decrease in CO uptake from 101 $\mu mol\,g^{-1}$ to 27 $\mu mol\,g^{-1}$ compared with the fresh sample, a 73% decrease in surface Ru sites. In contrast, the O_2 uptake from the fresh to spent $Ru_{18}Sn_5$/C samples only decreased by 15%, indicating that Ru centers were largely responsible for the initial activity in bimetallic catalysts with a low-Sn content, and deactivation was primarily associated with these sites.

The spent RuSn/C sample had a 38% decrease in CO uptake, indicating a significant decrease in the surface concentration of Ru surface atoms. Additionally, a 53% decrease in total O_2 uptake for the spent sample was observed. However, the stable level of activity with time on stream for this sample containing equal amounts of Ru and Sn suggests that large Ru ensembles did not contribute significantly to the activity of the RuSn/C catalyst, in view of the low surface Ru population indicated by CO chemisorption for the fresh catalyst.

In the case of $RuSn_4$/C, the CO uptake increased from 1 $\mu mol\,g^{-1}$ to 15 $\mu mol\,g^{-1}$ while the total O_2 uptake decreased 43%. These results suggest an increase in the Ru:Sn surface ratio, possibly caused by leaching of Sn from the sample. For all catalysts, the loss in activity could not be attributed to significant changes in the catalyst support, based on physisorption measurements of the spent samples.

4. Discussion

The observations of lower turnover frequencies, alongside improved selectivities toward LA hydrogenation with increasing Sn loadings, were primarily attributed to the formation of RuSn alloys, which had substantially lower activity for C=C hydrogenation and were more stable in the alkylphenol solvent. Previously Adams, et al. reported that the formation of Ru_xSn_y alloys significantly changed the selectivity of the catalyst during cyclododecatriene hydrogenation [29]. Although the compositions of alloys present were not measured, the phase diagram for the Ru–Sn system was used as a guide to suggest qualitatively how the experimental results from this study can be explained in terms of different behaviors for the various phases that may be present, Ru, Ru_xSn_y, and Sn. The phase diagram of Ru–Sn [30] at the reaction temperature of 453 K, shows 5 possible phase compositions, with 3 two-phase regions: monometallic Ru (occurs at 0 at% Sn), Ru plus Ru_2Sn_3 (0–60 at% Sn), Ru_2Sn_3 plus Ru_3Sn_7 (60–70 at% Sn), Ru_3Sn_7 plus a β-Sn phase (>71 at% Sn), and a monometallic β-Sn phase (100 at% Sn). Table 3 shows the relative proportions of the phases that are predicted to be present in the various Ru_xSn_y/C catalysts of this study.

Table 3
Phase compositions predicted for Ru_xSn_y/C catalysts as suggested from the binary alloy phase diagram of Ru–Sn at 453 K.

Sample	Sn (at%)	Phase composition			
		Ru (%)	Ru_2Sn_3 (%)	Ru_3Sn_7 (%)	β-Sn (%)
5% Ru/C	0	100	0	0	0
$Ru_{18}Sn_5$/C	21	65	35	0	0
RuSn/C	50	17	83	0	0
$RuSn_4$/C	80	0	0	69	31
18% Sn/C	100	0	0	0	100

The monometallic Ru/C catalyst showed the highest turnover frequency for hydrogenation of LA and SBP, but it also deactivated the most rapidly. The $Ru_{18}Sn_5$/C catalyst initially deactivated at a similar rate, but had a lower initial activity than the Ru/C catalyst. Both XRD and TEM/SEM showed insignificant changes in the size distributions of metal particles on pre- and post-reaction samples, indicating that sintering in the reaction environment was not the cause of the activity loss. The CO chemisorption measurements identified a loss of surface Ru density for both catalysts, and the loss of surface sites for the monometallic Ru/C catalyst agrees with the observed changes in hydrogenation rates as illustrated in Fig. 5a, but a significant amount of Ru did not leach from these catalysts. The initial rates in these samples are attributed to the Ru phase, and the loss of activity with time on stream is associated with a decrease in monometallic Ru sites due to coking. The results of physisorption measurements support this hypothesis, because the decrease in surface area and pore volume for the Ru catalyst before and after reaction was likely due to the coking. The $Ru_{18}Sn_5$/C catalyst is predicted to contain 65% monometallic Ru phase, which deactivates (Fig. 5a) with time on stream, and 35% of Ru_2Sn_3 phase that stabilizes at a low activity and does not hydrogenate the C=C present in the alkylphenol.

The RuSn/C catalyst is predicted to contain the same phases as the $Ru_{18}Sn_5$/C catalyst: monometallic Ru and Ru_2Sn_3, but at different percentages, over two times the amount of Ru_2Sn_3 than $Ru_{18}Sn_5$/C. After the catalysts stabilized, the RuSn/C catalyst was three times more active than the $Ru_{18}Sn_5$/C catalyst for LA hydrogenation and did not hydrogenate the SBP. Good metal dispersions were maintained as the amount of Sn is increased up to equimolar Ru:Sn loadings, and the monometallic Ru and Ru_2Sn_3 phases did not sinter significantly at the reduction and reaction conditions used.

At loadings higher than 60 at% Sn, the monometallic Ru phase does not exist, and Sn-rich phases are observed such as Ru_2Sn_3, Ru_3Sn_7, and β-Sn [30]. The $RuSn_4$/C catalyst is predicted to be approximately two-thirds Ru_3Sn_7 and one-third β-Sn phase (Table 3). At the reduction temperature of 723 K, the β-Sn undergoes a phase transformation to liquid Sn that readily sinters to form large particles, which were seen in the samples after reduction and passivation of the $RuSn_4$/C catalyst (Fig. 8d1). The β-Sn in the monometallic Sn/C catalyst behaved similarly under the reduction conditions as seen in Fig. 3c and d. After reaction, the atomic percent of Ru and Sn in the $RuSn_4$/C catalyst was closer to 33% and 66%, respectively (Fig. 9), due to leaching of the Sn phase. At 66 at% Sn, the two phases composing the catalyst would be two intermetallic Ru–Sn alloys, Ru_2Sn_3 (50%) and Ru_3Sn_7 (50%) [30]. These alloys appear to be active and stable in the hydrogenation of LA (C=O), but not in the hydrogenation of SBP (C=C). In addition, the impurities from corn stover and formic acid do not appear to inhibit significantly the catalytic properties of these Ru–Sn alloys.

5. Conclusions

The catalytic properties of Ru/C were modified significantly by the addition of Sn, leading to improved selectivity and stability in the hydrogenation of LA to GVL in presence of SBP solvent. The results from reaction kinetics studies, combined with results from electron microscopy studies and data from CO and O_2 chemisorption, suggested the presence of multiple metal phases: Ru, Ru_2Sn_3, Ru_3Sn_7, and β-Sn. The monometallic Ru phase was the most active; however, it undergoes deactivation (by coking) with time on stream and hydrogenated both the C=O bond in LA and the C=C bonds present in the alkylphenol solvent. The addition of Sn led to the formation of bimetallic Ru–Sn alloys, such as Ru_2Sn_3 and Ru_3Sn_7. These alloys had lower turnover frequencies for hydrogenation reactions compared to the monometallic Ru phase, but showed improved stability versus time on stream, and improved selectivity for hydrogenation of LA versus the SBP solvent. Increasing the amount of Sn created an additional phase, β-Sn, that was not active in the hydrogenation reactions, sintered readily, and leached under reaction conditions. Among the catalysts studied, $RuSn_4$/C proved to be stable even using LA produced from real biomass, corn stover, demonstrating that it is a promising catalyst to produce valuable chemicals and fuels from real biomass.

Acknowledgments

This work was supported in part by the U.S. Department of Energy Office of Basic Energy Sciences, and by the DOE Great Lakes Bioenergy Research Center (www.greatlakesbioenergy.org), which is supported by the U.S. Department of Energy, Office of Science, Office of Biological and Environmental Research, through Cooperative Agreement between The Board of Regents of the University of Wisconsin System and the U.S. Department of Energy. In addition, this work was supported by the Defense Advanced Research Projects Agency (DARPA) and Army Research Lab (ARL) through the Defense Science Office Cooperative Agreement W911NF-09-2-0010/09-005334 B 01 (Surf-Cat: Catalysts for production of JP-8 range molecules from lignocellulosic biomass). The views, opinions, and/or findings contained in this article are those of the authors and should not be interpreted as representing the official views or policies, either expressed or implied, of the Defense Advanced Research Projects Agency or the Department of Defense.

References

[1] J.C. Serrano-Ruiz, D.J. Braden, R.M. West, J.A. Dumesic, Appl. Catal. B: Environ. 100 (2010) 184–189.
[2] J.C. Serrano-Ruiz, D. Wang, J.A. Dumesic, Green Chem. 12 (2010) 574–577.
[3] L. Deng, J. Li, D.M. Lai, Y. Fu, Q.X. Guo, Angew. Chem. Int. Ed. 48 (2009) 6529–6532.
[4] I.T. Horvath, H. Mehdi, V. Fabos, L. Boda, L.T. Mika, Green Chem. 10 (2008) 238–242.
[5] L. Deng, Y. Zhao, J.A. Li, Y. Fu, B. Liao, Q.X. Guo, ChemSusChem 3 (2010) 1172–1175.
[6] H. Heeres, R. Handana, D. Chunai, C.B. Rasrendra, B. Girisuta, H.J. Heeres, Green Chem. 11 (2009) 1247–1255.
[7] Z.P. Yan, L. Lin, S.J. Liu, Energy Fuel 23 (2009) 3853–3858.
[8] X.L. Du, L. He, S. Zhao, Y.M. Liu, Y. Cao, H.Y. He, K.N. Fan, Angew. Chem. Int. Ed. 50 (2011) 7815–7819.
[9] J.J. Bozell, L. Moens, D.C. Elliott, Y. Wang, G.G. Neuenscwander, S.W. Fitzpatrick, R.J. Bilski, J.L. Jarnefeld, Resour. Conserv. Recycl. 28 (2000) 227–239.
[10] S.W. Fitzpatrick, Feedstocks for the Future, American Chemical Society (2006) 271–287.
[11] I.T. Horvath, Green Chem. 10 (2008) 1024–1028.
[12] H. Mehdi, V. Fabos, R. Tuba, A. Bodor, L.T. Mika, I.T. Horvath, Top. Catal. 48 (2008) 49–54.
[13] L.E. Manzer, Appl. Catal. A: Gen. 272 (2004) 249–256.
[14] J.P. Lange, J.Z. Vestering, R.J. Haan, Chem. Commun. (2007) 3488–3490.
[15] J.Q. Bond, D.M. Alonso, D. Wang, R.M. West, J.A. Dumesic, Science 327 (2010) 1110–1114.
[16] J.-P. Lange, R. Price, P.M. Ayoub, J. Louis, L. Petrus, L. Clarke, H. Gosselink, 4479-4483, Angew. Chem. Int. Ed. 49 (2010), S4479/4471-S4479/4474.
[17] J.Q. Bond, D. Martin Alonso, R.M. West, J.A. Dumesic, Langmuir 26 (2010) 16291–16298.
[18] J.Q. Bond, D. Wang, D.M. Alonso, J.A. Dumesic, J. Catal. 281 (2011) 290–299.
[19] H. Chen, B. Yu, S. Jin, Bioresour. Technol. 102 (2011) 3568–3570.
[20] J. Hegner, K.C. Pereira, B. DeBoef, B.L. Lucht, Tetrahedron Lett. 51 (2010) 2356–2358.
[21] D.J. Braden, C.A. Henao, J. Heltzel, C.C. Maravelias, J.A. Dumesic, Green Chem. 13 (2011) 1755–1765.
[22] D.M. Alonso, S.G. Wettstein, J.Q. Bond, T.W. Root, J.A. Dumesic, ChemSusChem 4 (2011) 1078–1081.
[23] Z. Kowalczyk, S. Jodzis, W. Raróg, J. Zielinski, J. Pielaszek, A. Presz, Appl. Catal. A: Gen. 184 (1999) 95–102.
[24] I. Wachs, Characterization of Catalytic Materials, Momentum Press, New York, 1992.
[25] B. Bachiller-Baeza, A. Guerrero-Ruiz, I. Rodríguez-Ramos, Appl. Catal. A: Gen. 192 (2000) 289–297.
[26] Y. Pouilloux, F. Autin, C. Guimon, J. Barrault, J. Catal. 176 (1998) 215–224.
[27] M. d.C. Aguirre, P. Reyes, M. Oportus, I. Melián-Cabrera, J.L.G. Fierro, Appl. Catal. A: Gen. 233 (2002) 183–196.
[28] P. Chantaravitoon, S. Chavadej, J. Schwank, Chem. Eng. J. 98 (2004) 99–104.
[29] R.D. Adams, E. Trufan, Philos. T. Roy. Soc. A 368 (2010) 1473–1493.
[30] T.B. Massalski, L.H. Bennett, J.L. Murray, H. Baker, Binary Alloy Phase Diagrams, Metals Park, OH, 1986.